# Improving the visualization process for binary neutron star merger simulations

**David Littel**

**13981439**

Report Bachelor Project Physics and Astronomy

| | |
|---|---|
| Size | 15 EC |
| Conducted between | 12 April 2024 and 28 June 2024 |
| Research institute | Anton Pannekoek Institute (API) |
| Universities | University of Amsterdam & Vrije Universiteit Amsterdam |
| UvA Faculty | Faculteit der Natuurwetenschappen, Wiskunde en Informatica |
| VU Faculty | Faculteit Bètawetenschappen |
| Submission Date | 28 June 2024 |
| Daily Supervisor | Dr. Philipp Mösta |
| Supervisor | Dr. Philipp Mösta |
| Second Examiner | Prof. Dr. Sera Markoff |


## Summary

As part of the research project, the 3D-visualization package `FieldVis` was expanded with isosurface plots, vector arrow plots, and 2D-sliced vector streamline plots. These features were added to promote its usage within the research group of dr. Philipp Mösta by improving the flexibility of the package. The isosurface plots function as intended, but the vector field visualizations can still be improved as part of future research.

In addition to the Python-oriented part of the project, data from a general-relativistic magnetohydrodynamic simulation of a binary neutron star merger remnant was used to test approximations for the amount of material ejected from the system. Specifically, the geodesic criterion and variants of the Bernoulli criterion were compared for use in quantifying the amount of unbound material in the polar jets of a hypermassive neutron star merger remnant. Finally, the properties of these polar ejecta were investigated to determine if their properties match with the properties of the blue component observed in kilonova light curves from binary neutron star merger GW170817.

In the end, the most accurate criterion was found to be the Bernoulli criterion including r-process heating and neutrino cooling. The Bernoulli criterion can still be improved by taking into account the r-process heating timescale, which will further improve the accuracy of the criterion. The polar jets largely match the conditions observed in the blue kilonova component, but the matter in the simulation was ejected at slightly lower velocities compared to the inferred properties from observations. The origins of the blue component of a kilonova's light curve could be further narrowed down with new observations in the future.



## Samenvatting

In dit bachelorproject is het visualisatieprogramma `FieldVis` uitgebreid met nieuwe visualisatie-opties. Het is nu mogelijk om een oppervlak te laten tekenen op de rand van een neutronenster aan de hand van 3D-data die verkregen is uit computersimulaties. Ook is het nu mogelijk om de individuele onderdelen van het magnetische veld van zo'n simulatie weer te geven, zowel in 2D als 3D, maar dit onderdeel werkt nog niet perfect en kan in de toekomst verbeterd worden.

Dit programma is vervolgens gebruikt om de samensmelting van botsende neutronensterren te onderzoeken met behulp van simulatiedata. Neutronensterren zijn sterren die een heel hoge dichtheid hebben en bijna alleen uit neutronen bestaan. Als twee neutronensterren met elkaar samensmelten ontstaat er meteen een zwart gat of tijdelijk een neutronenster die na een korte tijd een zwart gat wordt. In het specifiek is de samenstelling van de materie uitgezonden na de botsing onderzocht. Na de botsing zorgt het extreem sterke magnetische veld van de nieuw gevormde neutronenster voor een stroom van materie die uitgezonden wordt bij de magnetische polen van de neutronenster.

In dit onderzoek is onderzocht of deze materie atoomkernen vormt van hoge of lage massa. Als er vooral atoomkernen van lage massa worden gevormd, zorgt dit voor een uitzending van ultraviolet en zichtbaar licht, maar als er zwaardere kernen worden gevormd wordt er vooral infrarood licht uitgezonden. Uit het onderzoek is gebleken dat het waarschijnlijk is dat de materie uitgezonden bij de magnetische polen lichtere atoomkernen vormt, en dus een mogelijke bron is van het ultraviolette licht dat wij hebben ontvangen vanaf samensmeltende neutronensterren[1].


[1] A translation has been provided for grading purposes, which can be found in appendix B.

# Contents

# Introduction

## Motivation

Binary neutron star mergers have become one of the most important astronomical events in our universe since their first observation in 2017, when the combined efforts of many researchers observed the merger GW170817 using both gravitational waves and telescopes covering the entire electromagnetic spectrum. These observations revealed that binary neutron star mergers are responsible for the nucleosynthesis of many of the heaviest elements in our universe. However, not all mechanisms driving the emission of electromagnetic radiation in these events are well understood. In addition, they are observed extremely rarely, so simulations play a large role in improving our understanding of the physics at play. It is therefore important that these simulations can be properly visualized to fully realize their potential.

The current standard for visualizing neutron star binary merger simulations in dr. Mösta's research group is a program called `VisIt`, which features a graphical user interface (GUI), many different plot types and supports a wide variety of data files. It is very useful for exploring 3D datasets, since plot settings can be changed on the fly and the 3D plot window allows the user to move through and zoom in on points within the data. The downsides of this program are its slow loading times and issues with crashing; loading in data files can take minutes at a time. As a result, Nathanyel Schut developed a Python package called `FieldVis` as part of his bachelor project in 2022 as an alternative visualization tool specialized in visualizing the merger simulations done in the group, with the package `PyVista` as a rendering tool. This package remedied the slow loading times, loading and visualizing data in a matter of seconds, but offers less flexibility in both plot types and data types supported in the package. It utilizes `Jupyter` notebooks to set plot settings and generate 3D plots rather than a GUI, making it less user-friendly than `VisIt`. The limited flexibility has thus far hindered the adoption of `FieldVis` in the group, consequently this research project aims to improve the flexibility to hopefully replace `VisIt` in the near future.

## Theoretical background

In this section, theoretical information about binary neutron star mergers and related physical phenomena is provided to lay the groundwork for the research described in this paper.

### Binary Neutron Star Mergers

Binary neutron star (BNS) systems are usually formed from a binary system of high-mass main sequence stars that collapse into neutron stars through core-collapse supernovae without destabilizing the binary system, which is known as isolated classical binary evolution. According to research conducted by Belczynski, K. et al. (2018), this formation channel is about 100 times more common than BNS systems formed through globular cluster dynamics or nuclear cluster dynamics. They also found that 97% of BNS systems formed through isolated classical binary evolution merge within 1 Gyr of star formation, but more detailed estimates for the amount of time between BNS system formation and merging, also known as the delay time distribution, are difficult to make (Safarzadeh et al., 2019).

Even though the frequency of BNS mergers is not accurately known, the merger process itself is relatively well understood. The binary system's orbits are unstable and over time the neutron stars will spiral inwards around their center of mass until they eventually collide and merge. During this phase, gravitational waves are emitted, which can be observed on earth using gravitational wave detectors. After the merger, large amounts of matter are ejected from the system at high velocities through the transfer of angular momentum, which is referred to as

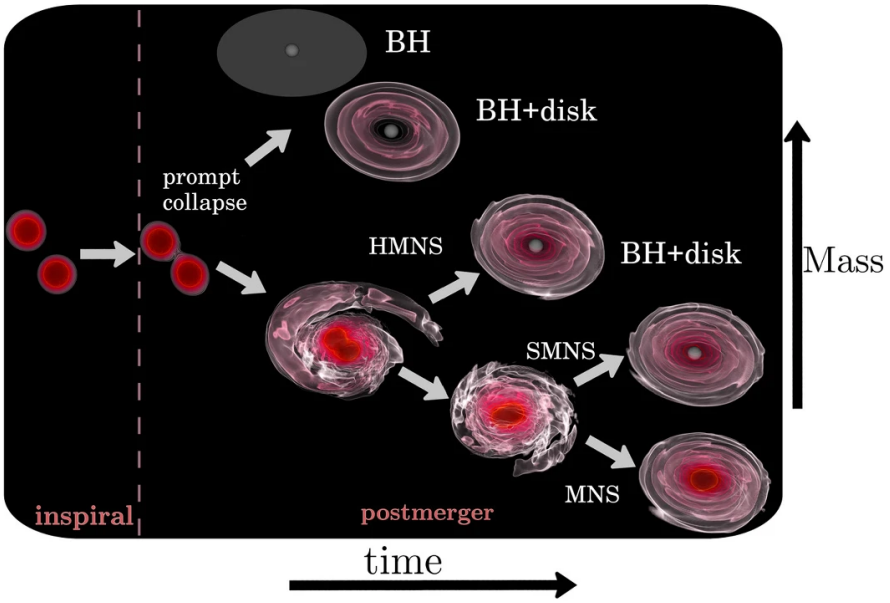


Figure 1: A schematic representation of the possible remnants of BNS mergers, from Dietrich et al. (2021). It shows that the remnant can either collapse immediately into a black hole with minimal ejected matter, or form various neutron star variants with different amounts of ejected matter en emitted light, depending on the total mass present in the BNS system.

the dynamical ejecta. These ejecta are responsible for most of the light we observe from these mergers and synthesize many of the heaviest elements present in our universe; the sections about kilonovae and the r-process will elaborate on these phenomena.

A schematic view of the possible post-merger objects is shown in figure 1 (Dietrich et al., 2021). If the pre-merger neutron stars are especially massive, with total mass above $\sim 2.8 M_{\odot}$, the merger remnant might immediately collapse into a black hole, but usually the total mass is lower, at around $\sim 2.75 M_{\odot}$, resulting in a neutron star merger remnant (Shibata and Hotokezaka, 2019). This merger remnant features an accretion torus and magnetic field strength on the order $B \sim 10^{15} G$. They can be classified as hypermassive (HMNS), supramassive (SMNS) or simply massive (MNS), depending on the baryonic mass. HMNS remnants typically collapse into a black hole within $\sim 10 - 20$ ms due to their large masses (Shibata and Hotokezaka, 2019). SMNS remnants have been shown to collapse quickly after their formation: they are theorised to emit electromagnetic radiation much more intensely then their HMNS and MNS counterparts; these emissions are observed much less frequently than predicted, implying that some mechanism causes them to collapse before they can emit much radiation (Wang et al., 2023). If the neutron star remnant's mass is low enough, it could be stable for a longer period of time or simply not collapse at all and become a regular neutron star (Dietrich et al., 2021).

Beyond the initial dynamical ejecta, HMNS remnants can also eject matter through the magnetic poles using their strong magnetic fields (de Haas et al., 2024). These polar jets are similar to the dynamical ejecta in many ways: they are ejected at high velocities, they feature r-process nucleosynthesis and drive kilonova emissions. It is theorised that the kilonova emissions from the polar jets peak earlier at ultraviolet wavelengths, while the kilonova emissions from the dynamical ejecta peak later and at infrared wavelengths, which will be discussed in the section about kilonovae.

### R-process

During the BNS merger aftermath, many heavy elements are synthesized. This fusion functions differently from nuclear fusion in main sequence stars. Instead of fusing multiple nuclei together, heavier nuclei are formed by capturing neutrons from the environment; this can only occur in extreme environments like post-merger ejecta or core collapse supernovae, since free neutrons are usually too unstable to exist and will quickly decay to protons and electrons, making r-process fusion impossible. When stable nuclei capture free neutrons, they become radioactive isotopes as a result. If these isotopes then decay through $\beta^-$-decay, a nucleus with more protons is formed, effectively becoming a heavier element.

In theory there is no limit to the mass of elements that can be created through this process, but in BNS merger remnant environments, the highest mass of nuclei that can be formed through r-process nucleosynthesis is determined by the electron fraction (Curtis et al., 2022). The electron fraction is a quantity which represents the neutron-richness of a piece of matter:

$$Y_e = \frac{n_p}{n_n + n_p}, \tag{1}$$

where $n_p$ and $n_n$ is the number of protons and neutrons respectively. From equation 1 it is obvious that lower values of $Y_e$ indicate a more neutron-rich environment.

In their paper "*r-process nucleosynthesis and kilonovae from hypermassive neutron star post-merger remnants*", Curtis et al. (2022) present the abundances of nuclei formed through the r-process in BNS merger remnant ejecta, based on the electron fraction of the ejected material[2]. They found that for $Y_e$-values below 0.2 result in r-process fusion of elements with high mass numbers $A \gtrsim 140$, while $Y_e$-values between 0.25 and 0.4 result in r-process fusion of elements with lower mass numbers $A \lesssim 140$. For higher electron fractions, they found only weak r-process fusion, resulting in a composition dominated by Fe-nuclei.

The dynamical ejecta of BNS merger remnants have been observed to feature very low electron fractions, likely being responsible for many of the heaviest elements in our universe: the abundance of higher mass elements obtained from simulated dynamical ejecta match up closely with the abundances in the sun (Radice et al., 2016). The polar ejecta typically feature less neutron-rich material, with higher average electron fractions than the dynamical ejecta (Curtis et al., 2022). The difference in composition have been proposed as a possible cause for the differences between the kilonova emissions associated with these ejecta, which will be elaborated upon in the next section.

### Kilonovae

Kilonova explosions are some of the most important observable phenomena resulting from binary neutron star mergers, next to gravitational waves and short Gamma Ray Bursts. They are especially useful for inferring physical properties of the material ejected from binary neutron star merger systems, because kilonova emissions are driven by the radioactive decay of unstable isotopes present in these ejecta. Therefore, the observed radiation from kilonovae provides us with ample information about the composition of the ejecta.

For example, the first kilonova explosion was observed in 2017 after the detection of gravitational waves pointed us towards the neutron star binary merger GW170817, which was observed in a wide variety of wavelength bands using many different telescopes, as can be seen in figure 2. This figure shows combined light curves from most of the observations of GW170817, compiled into a single plot by Villar et al. (2017), where the x-axis counts days since the merger.

[2]Specifically the abundances observed for the r-process in the polar ejecta of a HMNS remnant.

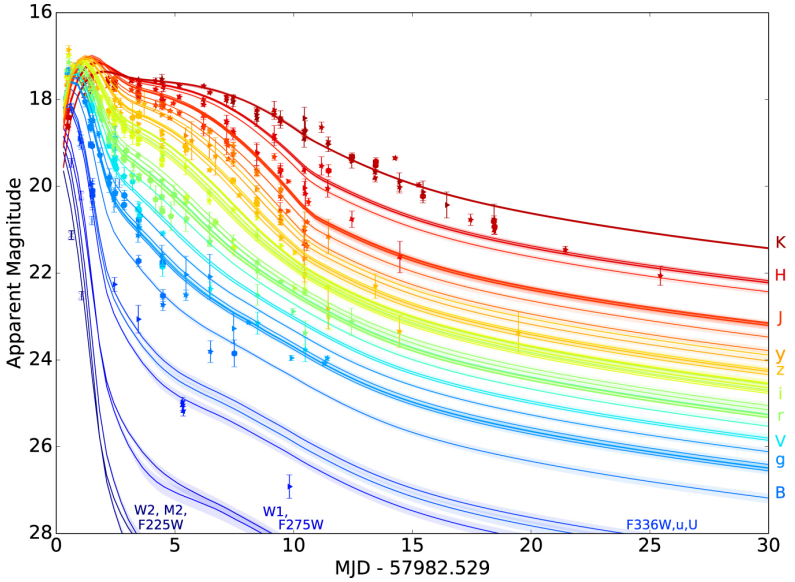


Figure 2: The kilonova light curve of BNS merger GW170817, compiled from many different observations by Villar et al. (2017) in 2017. Several emission components can be identified in this figure, but most significant are the drawn out component which loses its magnitude slowly, usually called the "red" component and the component losing its magnitude over a few days, especially visible in the ultraviolet filters W1 and W2, usually called the "blue" component.

The light curve can be roughly divided in two or three components, but mostly a longer lasting, brighter "red" component covering large parts of the infrared and optical spectrum and the short-lived "blue" component, which covers not only the infrared and optical spectrum, but also ultraviolet frequency ranges, where it can be clearly seen in the W1 and W2 filters decaying over a few days. According to Villar et al. (2017), the blue component is emitted by ejecta composed mostly of lower mass elements with mass numbers $A \lesssim 140$, because elements of higher mass, such as lanthanides, would absorb the ultraviolet wavelengths. Inversely, the red component includes elements of mass $A \gtrsim 140$, which block the ultraviolet part of the light curve, resulting in an infrared-dominated emissions spectrum.

The red component's origin point is generally well understood, most likely being emitted from the dynamical ejecta of the BNS merger and outflows from the merger remnant's accretion torus, while the blue component's origins are less certain (Curtis et al., 2022). The polar jets are a logical candidate, since simulations have shown that they could match the conditions observed in GW170817 and they represent a sufficiently large amount of the ejected matter (Curtis et al., 2022, Metzger et al., 2018). However, other options have also been proposed, such as winds driven by spiral density waves (Nedora et al., 2019), dynamical polar ejecta heated by the post-merger shockwave (Curtis et al., 2022), and winds driven by neutrino heating (Fahlman and Fernández, 2018).

### Approximating Unbound Material

When simulating binary neutron star mergers it is important to accurately quantify the outflow of matter from the neutron star remnant, since this ejected matter drives the emission of kilonovae. Whether a piece of matter near the remnant escapes the system can be determined using the

Lorentz factor. In special relativity, the Lorentz factor is calculated using the velocity relative to some reference frame:

$$\gamma = \frac{1}{\sqrt{1-\beta^2}},\ \beta = \frac{v}{c}, \tag{2}$$

The Lorentz factor at infinity, or asymptotic Lorentz factor, provides information about ejecta by revealing the theoretical velocity of that piece of ejecta at infinity. If this velocity were to be greater than zero, the ejecta would have escaped the gravity of the remnant and still be moving away from the system, and it should be classified as unbound matter. So, if the asymptotic Lorentz factor would be greater than one, this would imply that the asymptotic velocity would be nonzero relative to the remnant, therefore deriving an approximation for the asymptotic Lorentz factor is a powerful way to determine whether ejected matter will be unbound or fall back into the remnant.

However, this is easier said than done, since any approximation would need to take into account general relativity due to the extreme density of the BNS merger remnant, which is why no explicit derivations will be offered for the criteria discussed here. The simplest approximation would include only the curvature of space-time near the remnant and the velocity of the ejecta. This quantity is known as the geodesic criterion and it is given by the expression:

$$\Gamma_\infty = -u_t, \tag{3}$$

where $u_t$ is the time component of the general relativistic velocity four-vector (Hotokezaka et al., 2013, Foucart et al., 2021). This vector component is calculated with a combination of general relativistic quantities:

$$u_t = \frac{(g_{xx}v_x + g_{xy}v_y + g_{xz}v_z)\beta_x + (g_{xy}v_x + g_{yy}v_y + g_{yz}v_z)\beta_y + (g_{xz}v_x + g_{yz}v_y + g_{zz}v_z)\beta_z - \alpha}{\sqrt{1-(g_{xx}v_x + g_{xy}v_y + g_{xz}v_z)v_x - (g_{xy}v_x + g_{yy}v_y + g_{yz}v_z)v_y - (g_{xz}v_x + g_{yz}v_y + g_{zz}v_z)v_z}}, \tag{4}$$

where $g_{nm}$ are matrix elements of the metric from general relativity, $v_n$ are velocity components, and $\beta_n$ and $\alpha$ are given by:

$$\beta_n = \frac{v_n}{c};\ \alpha = \sqrt{1-\beta^2}. \tag{5}$$

A more complex approximation for the Lorentz factor is a quantity derived from hydrodynamics, called the Bernoulli criterion, which also takes into account the internal energies of the fluid, such as the pressure, temperature and density (Fujibayashi et al., 2020, Foucart et al., 2021). Technically, the matter ejected by BNS merger remnants is not a fluid, but it behaves similarly, so the Bernoulli criterion can still be used in this case. This criterion should offer a better estimate than the geodesic criterion when investigating the post-merger polar jets, since large parts of their total energy come from non-kinetic components (Foucart et al., 2021). The first version of the Bernoulli criterion takes on a similar form to the geodesic criterion:

$$\Gamma_\infty = \frac{-hu_t}{h_\infty}, \tag{6}$$

where $h$ and $h_\infty$ are the fluid's current enthalpy and asymptotic enthalpy respectively, given by:

$$h = 1 + \epsilon + \frac{P}{\rho}, \tag{7}$$

with $\epsilon$ the internal energy of the fluid, accounting for its thermal energy, nuclear binding energy and more, $P$ its pressure, which includes both thermodynamic pressure and magnetic field pressure, and $\rho$ the density of the fluid. Usually, the assumption is made that $h_\infty$ is equal to 1, resulting

in a much simpler calculation process. The accuracy of this assumption was investigated by Foucart et al. (2021), who found that the assumption is not accurate when assuming the matter's composition stays constant, but when accounting for energy released by r-process nucleosynthesis in the ejecta, it is remarkably accurate. They found the asymptotic enthalpy $h_\infty$ becomes $\sim 1$ for the DD2 and SFHo equations of state and $\sim 0.992$ for the LS220 equation of state, all of which are commonly-used equations of state within simulations. So the Bernoulli criterion accounting for r-process heating simply becomes:

$$\Gamma_\infty = -hu_t. \tag{8}$$

Another process Foucart et al. (2021) account for in their research is neutrino cooling. During r-process nucleosynthesis, the ejecta should radiate away energy in the form of neutrinos, causing a loss of energy which could in turn cause the material to fall back into the remnant. The full expression for the Bernoulli criterion including both r-process heating and neutrino cooling is:

$$\Gamma_\infty = -hu_t(0.9968 + 0.0085Y_e), \tag{9}$$

where $Y_e$ is the electron fraction of the ejecta. Finally, it is also possible to account for the heating timescale of the r-process in ejecta, since some matter might not fuse quickly enough to generate enough excess energy to escape the system. This final improvement was not implemented in this research and could be investigated further in the future.

### Research Objectives

The first goal for the research project was to update and expand the functionality of the `FieldVis` package. The most requested feature for the package was isosurface plotting[3], which could be used to visualize the edge of a star or accretion torus.

The second goal for the research project was to investigate the properties of material being ejected at the poles of a BNS merger remnant by leveraging simulation data obtained by other staff members of API. Specifically, the geodesic criterion and variants of the Bernoulli criterion were implemented and compared, and the composition of the ejected matter was researched to infer properties of the kilonova emissions that could originate from the polar jets.

## Methodology

### FieldVis Package Structure and Expansion

The `FieldVis` package contains three different Python scripts: `et_reader.py`, `field_dp.py`, and `field_plot.py`. The functions in `et_reader.py` serve as data readers which convert raw simulation data into `Numpy` arrays which are compatible with the package's functions; this script was not modified as part of the project. `field_dp.py` processes the input data into the correct data structure ready to be plotted using functions from `field_plot.py`. For example, when plotting magnetic field streamlines, `field_dp` takes the input list containing three 3D `Numpy` arrays and processes it into a `PolyData` class from `PyVista` that is compatible with the plotting functionality. A new function was added to `field_dp.py` called `get_arrows`, which creates an `ImageData` class storing vector field data, which can later be plotted using `field_plot.py`

The most important `field_plot.py` functions are: `plot_slice`, `plotter`, and `animator`. `plot_slice` takes a 2D slice of a scalar field and plots it using the package `Matplotlib`; this

[3] An isosurface is a surface in 3D space where the value of a scalar field is constant at every point of the surface.

was expanded to be compatible with vector field data. `plotter` takes data processed in the `field_dp.py` file and renders it using the `Plotter` function from `PyVista`; this function was expanded with isosurface plotting functionality and more vector field plotting options. The `animator` function uses the `plotter` function to render many frames at once without user input, allowing for the creation of animations from simulation data, as long as all settings are configured properly; this function was not expanded in this project. After implementation, the new plotting options in the package were tested using simulation data obtained from a simulation of a HMNS remnant.

For a more in-depth explanation of the package's structure and inner workings, readers are referred to Nathanyel Schut's thesis, which can be found on his github page: https://github.com/nathanyelschut/Visualization-of-binary-neutron-star-merger-simulations.

### Simulation Data

Simulation data obtained from a general-relativistic magnetohydrodynamic (GRMHD) simulation of a BNS merger remnant was used to test the newly implemented functionality of the `FieldVis` package. This simulation ran from shortly after the merger until the remnant collapsed into a black hole, spanning roughly 15 ms in time. The initial conditions for the simulation were created by taking the results of an earlier simulation, which ran up until the merger, and adding a poloidal magnetic field of $10^{15}G$. The data from three timepoints was used for this research, namely iteration numbers 18432, 36352, 53760, corresponding to 4.1 ms, 8.1 ms, and 11.9 ms after the simulation's start respectively. These correspond to time points approximately at the start, in the middle and near the end of the simulation.

### Data Analysis

Three different criteria were used to approximate the amount of unbound matter in the data: the geodesic criterion, the Bernoulli criterion with r-process heating and the Bernoulli criterion with r-process heating and neutrino cooling. The geodesic criterion was chosen since it is the simplest approximation, and it is still frequently used in the field. The two Bernoulli criteria were chosen because the r-heating variant is commonly used in dr Mösta's research group and the goal was to investigate whether implementing neutrino cooling offers a significant difference in the predicted amount of ejected matter.

Initially, all datasets were processed using a modified pre-existing Python script that calculates the geodesic criterion and both Bernoulli criterion variants and compiles them into a single data file per iteration. Then, the data files were loaded into a `Jupyter` notebook to visualize the results with the updated `FieldVis` package. In addition, the processed simulation data was compiled into a set of histograms which were used to compare the composition of the ejecta to the inferred properties of the blue kilonova component observed in actual binary neutron star mergers, in particular the merger observed in 2017, GW170817. These histograms were also compared to the results obtained by Curtis et al. (2024), since their research also investigated the polar ejecta as a source for the blue kilonova component.

## Results

In this section, the results of the `FieldVis` update and the results of the different criteria applied on the simulation data are presented.

## FieldVis Updates

The first step in improving the `FieldVis` package was updating all packages to their newest versions, since they were missing two years of updates. This involved some minor changes, such as changing any use of the `PyVista` class `UniformGrid` to `ImageData`, since this class was renamed. In addition, some minor bugs were fixed; one example is the `plot_slice` function plotting the data rotated 90 degrees relative to the axis labels.

I also found that the animator function in the package wasn't working on my Windows desktop. This was caused by the package `multiprocessing`, which is not compatible with `Jupyter` notebooks on Windows, replacing it with another package called `multiprocess` fixed the function for use with Windows, but might break Linux and MacOS functionality.

### Isosurface Plotting

The first new feature implemented in `FieldVis` was an expansion for the scalar field plotting, providing isosurface plotting as an alternative to volume plots. The implementation of isosurface plotting was relatively simple, since the infrastructure used for volume plotting mostly makes use of the `PyVista` class `ImageData`, which essentially stores the entire scalar field, and only during the final plotting step the type of plot needs to be specified. This is useful since it minimizes the performance impact and doesn't expand the code massively, which retains the readability of the original code, allowing for simpler updates in the future. Isosurface plotting can be enabled using a new keyword argument `volume_or_isosurface`, which uses a string for the user to specify whether they want to plot isosurfaces or volumes or both. Another two keyword arguments were introduced to customize the plotted isosurfaces: the `isosurface_thresholds` keyword specifies the values in the scalar field where isosurfaces should be plotted, and the keyword `isosurface_opacity` specifies the opacity for the isosurfaces, which is useful if both types of plots are used simultaneously.

An example of the isosurface functionality is shown in figure 3, where a singular isosurface is plotted representing the edge of the merger remnant, which is the main use for this functionality. The other subplot showcases the option for multiple isosurfaces, created by specifying multiple values in the isosurface_thresholds keyword. This new feature works very well and is used throughout the rest of this paper to indicate the location of the merger remnant in other plots.

### Vector Field Visualisation

After implementing isosurface plotting, I started working on expanding the vector field visualization possibilities. The first approach is visualizing the vector field using three-dimensional arrows, which could be useful to view the structure of the magnetic field around the remnant. When using this function, all arrows are plotted at the same size, which is supposed to help in cases where the magnetic field strength covers several orders of magnitude. Alternatively, logarithmic scaling could be implemented in the future along with colormap functionality, but during my testing I could not find settings that worked well with logarithmic scales.

Three examples of vector field arrow plots can be found in figure 4. The first subplot shows the full magnetic field at points where its magnitude is at least 0.5% of the largest magnitude in the dataset. Filtering vectors by their magnitude is achieved using the keyword `mask_thresholds`, which is a tuple of the lower and upper bound for the vector magnitudes, specified as a fraction of the largest vector magnitude. The second and third subplots show the parts of the magnetic field where the arrows are either mostly horizontal or mostly vertical, which is determined by checking if the z-component of the magnetic field is greater than 0.5. This filtering can be enabled by setting the keywords `hide_vertical_vectors` and `hide_horizontal_vectors` to

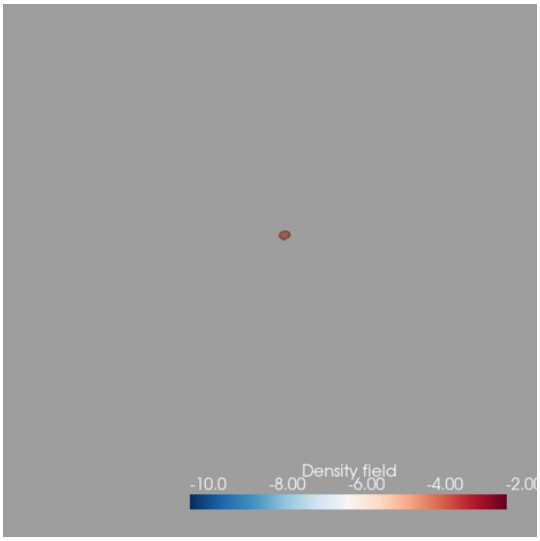


(a) The isosurface plotting feature used to plot the edge of the neutron star. The edge of the neutron star is approximated as a density of $10^{-3.50}$ in the simulation units; the scalar bar shows the density in logarithmic scale.

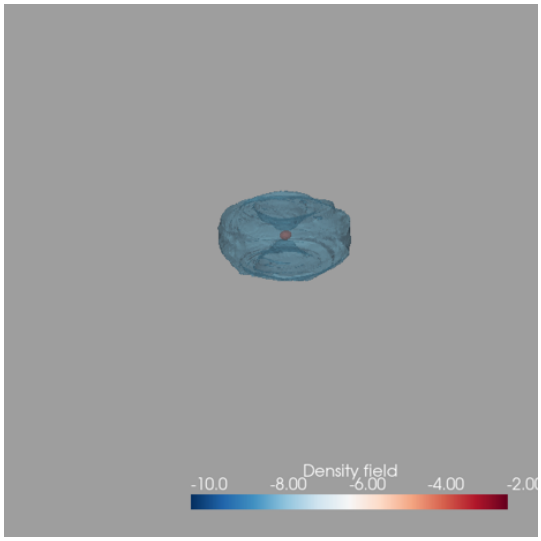


(b) The isosurface plotting feature used to plot multiple isosurfaces. Both the edge of the neutron star and its accretion torus are plotted. The isosurface of the accretion torus is plotted at a density of $10^{-8}$ in simulation units.

Figure 3: The newly implemented isosurface plotting feature used to visualize the BNS merger remnant.

True respectively. Separating the magnetic field like this helps reduce the clutter in the image, but the image is still very cluttered.

This visual clutter could be reduced using the built-in tolerance feature of the `PyVista` package, which sets the minimum distance between the individual arrows. Unfortunately, the algorithm that calculates the new vector field generated by this keyword slows down exponentially for higher values, so rendering less cluttered images can take minutes at a time, making it an unfavorable option for users. In addition, even with less arrows cluttering the area around the merger remnant, it can still be difficult to tell where the arrows are located in space, since there are no reference points in the figure beyond the core of the merger remnant. This could possibly be improved by adding some functionality that plots a uniform grid showing the space occupied by individual arrows, or by using an interactive plotting window supported by `PyVista`.

As an alternative to this three-dimensional plotting option, the `plot_slice` function was expanded to also be compatible with vector field data. This new version of the function takes either a list of a single `Numpy` array or a list of three `Numpy` arrays as input to distinguish between scalar and vector field plotting. When receiving a list with three elements, the function slices the data at the point requested by the user and plots the vector field projected onto the two-dimensional plane.

The plot shows streamlines of the vector field, with a colormap functionality which indicates the magnitude of the original three-dimensional vector, some examples are presented in figure 5. Subplot (a) shows the magnetic field from a top down view at the height of the merger remnant. It clearly shows the spiralling field lines near the remnant which vary a lot in strength; the spiral shape is caused by the rapid rotation of the merger remnant. Examining the other two subplots reveals an interesting issue: the sliced magnetic field seems to indicate that the magnetic

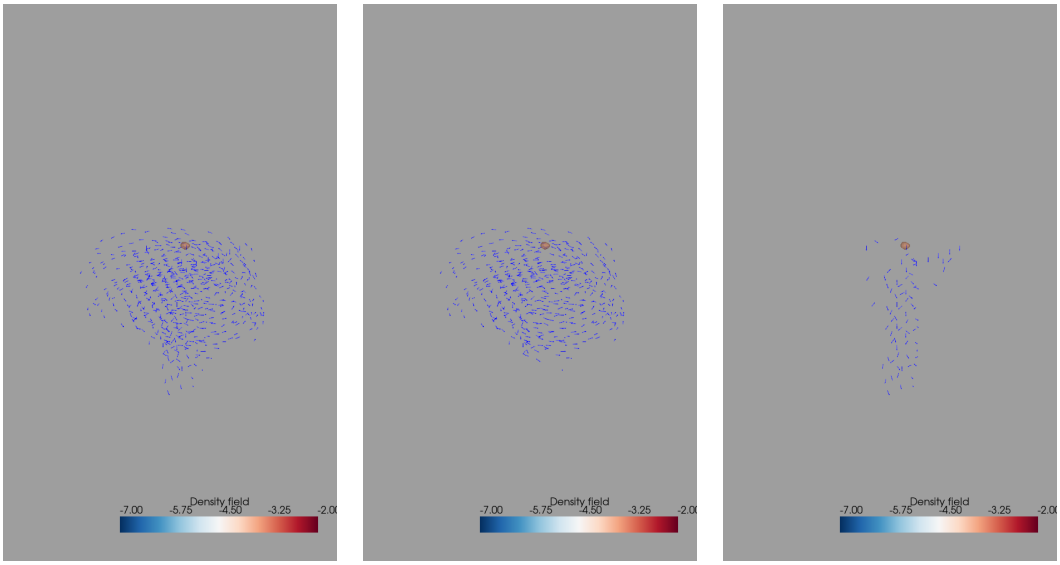


(a) The full magnetic field visualized using vector arrows

(b) The horizontal components of the magnetic field

(c) The vertical components of the magnetic field

Figure 4: The magnetic field of the BNS merger remnant, visualized using the new `FieldVis` vector arrow plot functionality. The arrows are displayed at a constant size, resulting in a cluttered image where it is hard to tell the exact location of individual arrows. Subplots featuring filtered versions of the magnetic field are also presented.

field is not axisymmetric, since the two plots look drastically different. When looking at the three-dimensional magnetic field in figure 4, there is no noticable difference in the magnetic field depending on the slice axis, so this asymmetry is likely an issue with the conversion from three-dimensional to two-dimensional vectors or some other part of the `slice_plot` function.

It is also noteworthy that the magnetic field sliced along the y-axis suggests that all field lines neatly flow outwards towards the edge of the grid. Comparing again to the three-dimensional visualization, this does not match up at all, since these field lines should be spiralling around the merger remnant. The cause for this is unknown, possibly the field lines in the y-slice happen to line up barely well enough to convince `Matplotlib` to connect the streamlines in this manner, but this seems unlikely. Perhaps this function could be re-examined in the future to improve the reliability; for now the 2D and 3D functions can be used in conjunction to understand the structure of magnetic fields or other vector fields.

## Visualized Simulation Data

The updated `FieldVis` functionality was used to visualize the post-processed simulation data in 3D, and a sample of these plots is shown in figures 6 and 7. All 3D plots created from this data can be found in appendix A at the end of the document. Figure 6 shows the evolution of the remnant and its jets over time. The remnant shrinks over time and the jets of ejected material become thinner, and show less intense color shades, corresponding to lower asymptotic Lorentz factors. The Lorentz factors were calculated using the Bernoulli criterion including r-process heating and neutrino cooling.

Figure 7 shows the three different criteria used to approximate the amount of unbound material

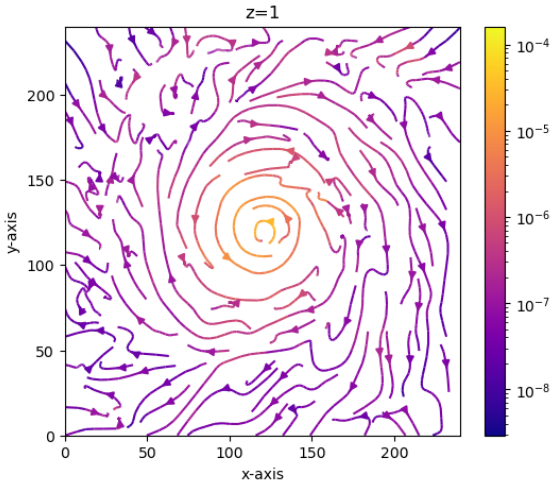


(a) The magnetic field sliced along the z-axis at the height occupied by the neutron star remnant.

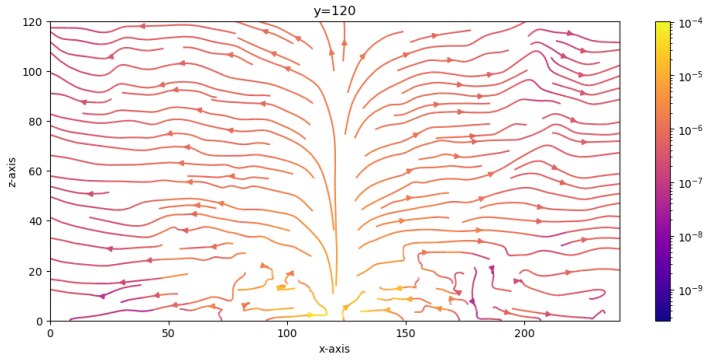


(b) The magnetic field sliced along the y-axis at the center of the grid occupied by the neutron star remnant.

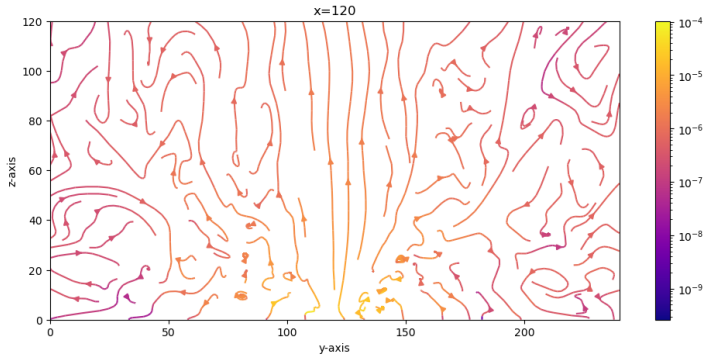


(c) The magnetic field sliced along the x-axis at the center of the grid occupied by the neutron star remnant.

Figure 5: The magnetic field of the BNS merger remnant sliced along different axes. The streamlines plotted in the x-sliced data and y-sliced data look very different, even though the remnant's magnetic field should be mostly axisymmetric.

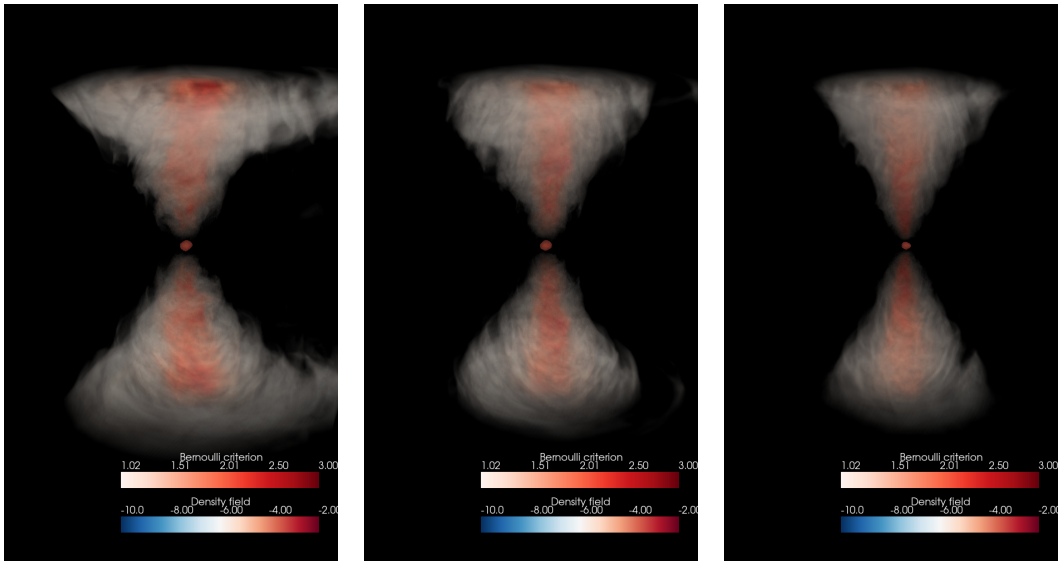


(a) t ≈ 4.1 ms (b) t ≈ 8.1 ms (c) t ≈ 11.9 ms

Figure 6: The Bernoulli criterion (with r-process heating and neutrino cooling) of the merger remnant over time, the jets of ejected material become thinner over time, implying less ejected matter over time. The merger remnant itself is also shrinking over time.

for one particular time step. The cone of unbound material predicted by the geodesic criterion is significantly smaller and has less intense color shading than both Bernoulli criterion variants. The differences between the two variants of the Bernoulli criterion used are not obvious from the volume plots; the amount of unbound mass predicted by each criterion for each timestep can be found in table 1. The geodesic criterion predicts significantly less unbound matter than the Bernoulli criterion, which is in line with findings from Foucart et al. (2021). Including neutrino heating in the Bernoulli criterion leads to $\sim 8\%$ less unbound matter early on in the simulation, but over time the difference between the criteria becomes smaller.

The processed data was also visualized using histograms to investigate the composition and velocity of unbound matter. Figure 8 shows the distribution of the radial velocity at which unbound matter was travelling at the time of the timesteps used. The geodesic criterion is in good agreement with the Bernoulli criterion for matter at higher velocities, but the Bernoulli criterion predicts more low-velocity ejecta, because these ejecta are more likely to require the extra energy included in the Bernoulli criterion to escape the remnant's gravity. Over time, the ejecta shift slightly toward higher velocities, indicating that the smaller cones observed in figure 6

Table 1: Unbound material masses by iteration number and criterion. The last column shows the percentage of matter which is predicted to be unbound by the criterion without cooling, but not by the criterion with cooling.

| Simulation time | $M_{\text{ej,geodesic}}$ $(10^{-4}\text{M}_\odot)$ | $M_{\text{ej,heating}}$ $(10^{-4}\text{M}_\odot)$ | $M_{\text{ej,heating+cooling}}$ $(10^{-4}\text{M}_\odot)$ | $\Delta M_{\text{ej}}(\%)$ |
|---|---|---|---|---|
| 4.1 ms | 0.620 | 2.28 | 2.09 | 8.33% |
| 8.1 ms | 0.903 | 2.28 | 2.15 | 5.70% |
| 11.9 ms | 0.314 | 1.34 | 1.30 | 2.99% |

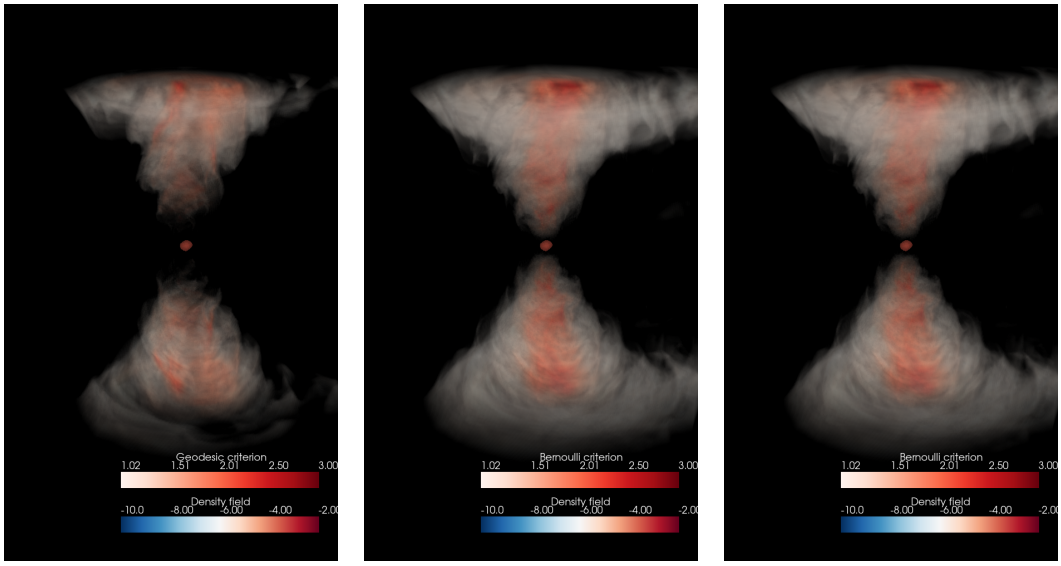


(a) Geodesic

(b) Bernoulli without neutrino cooling

(c) Bernoulli with neutrino cooling

Figure 7: Simulation data from t $\approx$ 4.1 ms, showing ejected material by criterion. The geodesic criterion shows an overall smaller cone and lower average values for the Lorentz factor. Both the Bernoulli criteria with and without cooling look similar to each other with no clear differences.

show a more concentrated jet of ejected material.

Figure 9 shows the electron fraction of the unbound matter. Initially, the matter is ditributed evenly accross all electron fractions, including both neutron-rich and neutron-poor material. However, the amount of neutron-rich ejecta decreases over time, while slightly more neutron-poor matter is observed. This could imply that r-process fusion can form heavy nuclei ($A \gtrsim 140$) post-merger for a short time, but afterwards most of the matter features electron fractions $\sim 0.3 - 0.5$, implying weaker r-process nucleosynthesis.

# Discussion and Conclusion

In this section, the presented simulation results are interpreted and discussed more in-depth. Finally, some conclusions and future research opportunities are discussed.

## Analysis of Simulation Data

In figure 6, the cone of ejected matter became thinner and less total mass was ejected over time. In addition, the remnant itself shrinks in size in the last presented time step compared to the first, all of which implies that the remnant has started collapsing into a black hole by the final time step, causing increased gravity and thus less total ejected matter.

### Geodesic and Bernoulli Criteria

The unbound polar ejecta have lower velocities on average around $v^r \sim 0.20c$, as shown in figure 8; the outflows with lower velocities must feature a significant amount of non-kinetic energy,

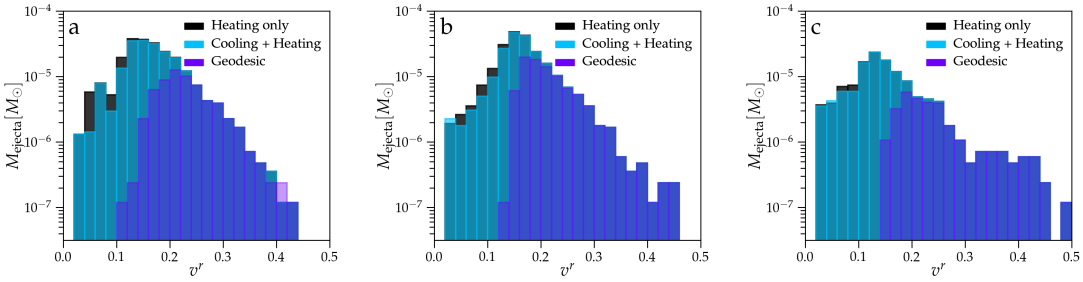


(a) t ≈ 4.1 ms (b) t ≈ 8.1 ms (c) t ≈ 11.9 ms

Figure 8: Histograms showing the distribution of the velocity of unbound matter by criterion. The geodesic criterion generally does well at predicting high-velocity ejecta, but the Bernoulli criterion also predicts more low-velocity ejecta. Over time, less low-velocity ejecta and slightly more high-velocity ejecta are observed.

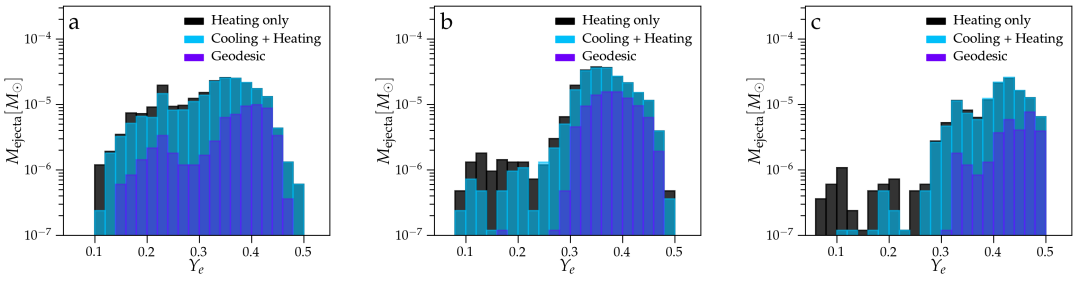


(a) t ≈ 4.1 ms (b) t ≈ 8.1 ms (c) t ≈ 11.9 ms

Figure 9: Histograms showing the distribution of the electron fractions of ejected matter. The three criteria are roughly the same in distribution, but the geodesic criterion predicts only high electron fractions later on, and much less ejected matter overall. The distribution is initially spread evenly over all values, but becomes concentrated at higher electron fractions later on.

which is why the Bernoulli criterion shows them as unbound while the geodesic criterion does not. The Bernoulli criterion is therefore a better approximation for the amount of unbound material than the geodesic criterion, because the Bernoulli criterion does well for predicting outflows with large amounts of non-kinetic energy. This supports the assessment from Foucart et al. (2021) that the Bernoulli criterion is better suited for approximated unbound material in outflows close to BNS merger remnants with large amounts of thermal energy, while the geodesic criterion is better for estimating outflows with large amounts of kinetic energy, such as the dynamical ejecta.

According to Foucart et al. (2021), the Bernoulli criterion usually overestimates the amount of ejected matter. Therefore, including r-process heating and neutrino cooling in the calculation of the Bernoulli criterion improves the accuracy of the predicted amount of unbound matter, since that amount is reduced by $\sim 3-8\%$, as shown in table 1. Using this version of the Bernoulli criterion would be advisable, since the electron fraction is usually already required for post-processing involving the criterion, and implementing the neutrino cooling term from equation 9 should then come at a negligible cost. Even though a difference of a few percentage points might not make a significant difference for the order-of-magnitude style calculations of observed kilonova light curves, the improved accuracy and small cost of implementation still make it a worthwhile addition. For the same reasons, the implementation of the r-process heating timescale detailed in Foucart et al. (2021) is likely also a good option to further improve the accuracy of the Bernoulli criterion.

### Blue Kilonova Component

According to Villar et al. (2017), the BNS merger GW170817 featured a blue kilonova component generated by a total mass of $M_{\text{ej}} \sim 0.020\text{M}_\odot$ and approximate velocity of $v^r \sim 0.27c$, which is described as a lanthanide-poor component, implying an electron fraction of $Y_e \sim 0.25-0.4$. In the dataset presented in this paper, the average velocities of the polar jets of $v^r \sim 0.20c$ are lower than the observed velocities in the kilonova, but the electron fraction during the later parts of the simulation peaks around $Y_e \sim 0.3-0.4$, implying that the composition of the jets could certainly match the material that created GW170817's blue kilonova component. Further post processing of the data presented here would lead to greater understanding of the composition and emitted light curve of this remnant, which could more conclusively determine whether the blue component originated from the polar ejecta, but there was no more time for this step in my research project. Perhaps a merger remnant with a stronger magnetic field could create polar jets of higher average velocity, leading to ejecta with features matching better with observed blue kilonova light curves.

Indeed, research published earlier this year has shown that polar ejecta matching the conditions by Villar et al. (2017) can be obtained using GRMHD simulations (Curtis et al., 2024). Comparing the results from this research with their results, the material is on average ejected slightly faster in their simulations, while the electron fractions observed are distributed similarly over time. They also found that the total mass of the polar ejecta can match the observed properties of the blue kilonova component, which is difficult to investigate in this research, since only three data points are available.

The findings from the simulation presented in this paper support the findings by Curtis et al. (2024); polar ejecta from HMNS merger remnants are prime candidates for the origin of the blue kilonova component.

## Conclusion

Over the course of this bachelor project, the functionality of the `FieldVis` package has been improved and greatly expanded, now featuring isosurface plotting, vector field arrow plots, and vector

field slice plots in addition to the previous options. The updated version of the FieldVis package can be found on my github account: https://github.com/lolhamster/Visualisation-Update Data obtained from GRMHD simulations has shown that the Bernoulli criterion including r-process heating and neutrino cooling offers improved accuracy in predicting unbound material from polar ejecta, compared to the traditional Bernoulli criterion and geodesic criterion. Its implementation is recommended for future research involving the polar jets of HMNS remnants, because the increase in accuracy outweighs the negligible cost in performance.

This research has also provided support for the polar jets as a source of a BNS merger's blue kilonova component, observing material ejected with similar properties to the observed blue component, with slightly lower average velocities but similar values for the electron fraction. The polar ejecta could be further researched by calculating the actual composition and expected light curve from the ejecta with more advanced post processing, instead of estimating the composition and light curve behavior using the electron fraction.

As part of future research, the `FieldVis` package could be expanded further, or the new vector field visualization options could be improved. In addition, the impact of the r-process heating timescale on the effectiveness of the Bernoulli criterion could be investigated. Finally, further research into the polar ejecta of BNS mergers is warranted when new data becomes available from observations to further investigate the viability of the polar jets as the origin of the blue kilonova component.

## Acknowledgements

I would like to thank dr. Philipp Mösta for the interesting project he offered me, and the support and guidance given throughout the project. I am also thankful for the rest of the research group for providing great feedback, especially for my presentation, and for fostering an open and welcoming environment, which helped me expand my knowledge of numerical astrophysics as a whole. Finally, I would like to thank Dr Pablo Bosch Gomez for providing me with the simulation data used for the research through cooperation with dr. Mösta.

## References

Belczynski, K., Askar, A., Arca-Sedda, M., Chruslinska, M., Donnari, M., Giersz, M., Benacquista, M., Spurzem, R., Jin, D., Wiktorowicz, G., & Belloni, D. (2018). The origin of the first neutron star – neutron star merger. *A&A*, *615*, A91. https://doi.org/10.1051/0004-6361/201732428

Curtis, S., Bosch, P., Mösta, P., Radice, D., Bernuzzi, S., Perego, A., Haas, R., & Schnetter, E. (2024). Magnetized Outflows from Short-lived Neutron Star Merger Remnants Can Produce a Blue Kilonova. *The Astrophysical Journal Letters*, *961*(1), Article L26, L26. https://doi.org/10.3847/2041-8213/ad0fe1

Curtis, S., Mösta, P., Wu, Z., Radice, D., Roberts, L., Ricigliano, G., & Perego, A. (2022). r-process nucleosynthesis and kilonovae from hypermassive neutron star post-merger remnants. *Monthly Notices of the Royal Astronomical Society*, *518*(4), 5313–5322. https://doi.org/10.1093/mnras/stac3128

de Haas, S., Bosch, P., Mösta, P., Curtis, S., & Schut, N. (2024). Magnetic field effects on nucleosynthesis and kilonovae from neutron star merger remnants. *Monthly Notices of the Royal Astronomical Society*, *527*(2), 2240–2250. https://doi.org/10.1093/mnras/stad2931

Dietrich, T., Hinderer, T., & Samajdar, A. (2021). Interpreting binary neutron star mergers: Describing the binary neutron star dynamics, modelling gravitational waveforms, and analyzing detections. *General Relativity and Gravitation*, *53*(3). https://doi.org/10.1007/s10714-020-02751-6

Fahlman, S., & Fernández, R. (2018). Hypermassive neutron star disk outflows and blue kilonovae. *The Astrophysical Journal Letters*, *869*(1), L3. https://doi.org/10.3847/2041-8213/aaf1ab

Foucart, F., Mösta, P., Ramirez, T., Wright, A. J., Darbha, S., & Kasen, D. (2021). Estimating outflow masses and velocities in merger simulations: Impact of $r$-process heating and neutrino cooling. *Phys. Rev. D*, *104*, 123010. https://doi.org/10.1103/PhysRevD.104.123010

Fujibayashi, S., Wanajo, S., Kiuchi, K., Kyutoku, K., Sekiguchi, Y., & Shibata, M. (2020). Postmerger mass ejection of low-mass binary neutron stars. *The Astrophysical Journal*, *901*(2), 122. https://doi.org/10.3847/1538-4357/abafc2

Hotokezaka, K., Kiuchi, K., Kyutoku, K., Okawa, H., Sekiguchi, Y.-i., Shibata, M., & Taniguchi, K. (2013). Mass ejection from the merger of binary neutron stars. *Physical Review D*, *87*(2). https://doi.org/10.1103/physrevd.87.024001

Metzger, B. D., Thompson, T. A., & Quataert, E. (2018). A magnetar origin for the kilonova ejecta in gw170817. *The Astrophysical Journal*, *856*(2), 101. https://doi.org/10.3847/1538-4357/aab095

Nedora, V., Bernuzzi, S., Radice, D., Perego, A., Endrizzi, A., & Ortiz, N. (2019). Spiral-wave wind for the blue kilonova. *The Astrophysical Journal Letters*, *886*(2), L30. https://doi.org/10.3847/2041-8213/ab5794

Radice, D., Galeazzi, F., Lippuner, J., Roberts, L. F., Ott, C. D., & Rezzolla, L. (2016). Dynamical mass ejection from binary neutron star mergers. *Monthly Notices of the Royal Astronomical Society*, *460*(3), 3255–3271. https://doi.org/10.1093/mnras/stw1227

Safarzadeh, M., Berger, E., Leja, J., & Speagle, J. S. (2019). Measuring the delay time distribution of binary neutron stars. iii. using the individual star formation histories of gravitational-wave event host galaxies in the local universe. *The Astrophysical Journal Letters*, *878*(1), L14. https://doi.org/10.3847/2041-8213/ab24e3

Shibata, M., & Hotokezaka, K. (2019). Merger and mass ejection of neutron star binaries. *Annual Review of Nuclear and Particle Science*, *69*(Volume 69, 2019), 41–64. https://doi.org/https://doi.org/10.1146/annurev-nucl-101918-023625

Villar, V. A., Guillochon, J., Berger, E., Metzger, B. D., Cowperthwaite, P. S., Nicholl, M., Alexander, K. D., Blanchard, P. K., Chornock, R., Eftekhari, T., Fong, W., Margutti, R., & Williams, P. K. G. (2017). The Combined Ultraviolet, Optical, and Near-infrared Light Curves of the Kilonova Associated with the Binary Neutron Star Merger GW170817: Unified Data Set, Analytic Models, and Physical Implications. *The Astrophysical Journal Letters*, *851*(1), Article L21, L21. https://doi.org/10.3847/2041-8213/aa9c84

Wang, H., Beniamini, P., & Giannios, D. (2023). Constraining the long-lived supramassive neutron stars by magnetar boosted kilonovae. *Monthly Notices of the Royal Astronomical Society*, *527*(3), 5166–5182. https://doi.org/10.1093/mnras/stad3560

# Appendices

## Appendix A: All 3D Plots

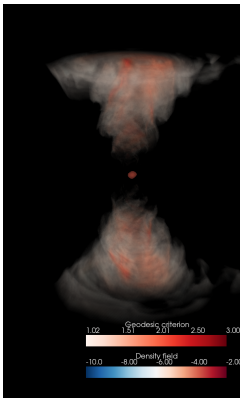

(a) t ≈ 4.1 ms, geodesic criterion

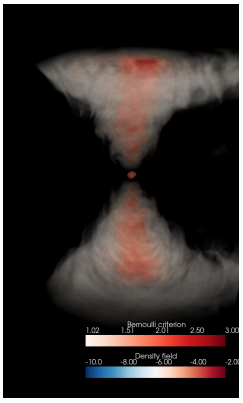

(b) t ≈ 4.1 ms, Bernoulli criterion, without cooling

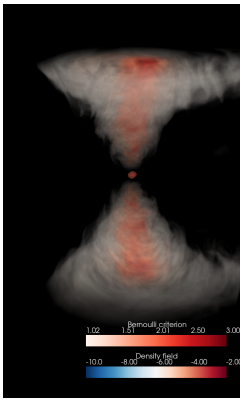

(c) t ≈ 4.1 ms, Bernoulli criterion, with cooling

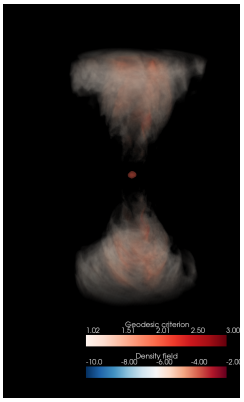

(d) t ≈ 8.1 ms, geodesic criterion

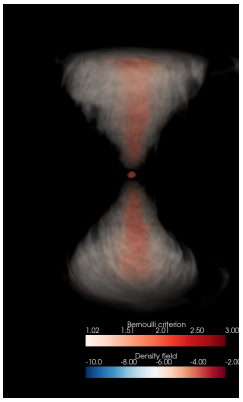

(e) t ≈ 8.1 ms, Bernoulli criterion, without cooling

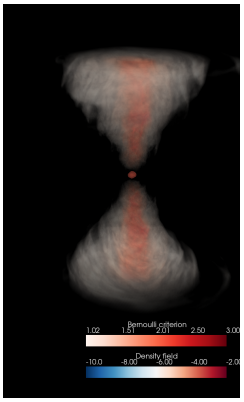

(f) t ≈ 8.1 ms, Bernoulli criterion, with cooling

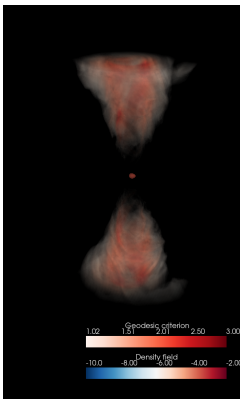

(g) t ≈ 11.9 ms, geodesic criterion

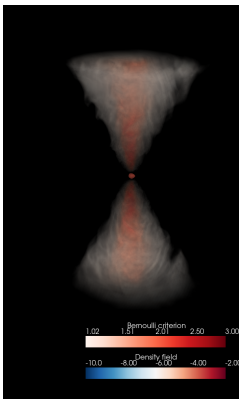

(h) t ≈ 11.9 ms, Bernoulli criterion, without cooling

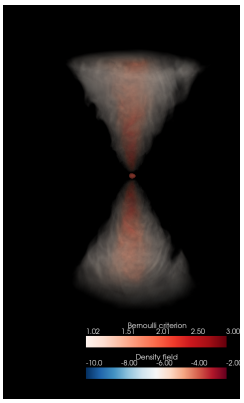

(i) t ≈ 11.9 ms, Bernoulli criterion, with cooling

Figure 10: All criterion variants plotted for every dataset.

## Appendix B: Popular Scientific Summary in English

In this bachelor project, the visualization program `FieldVis` was expanded with new visualization options. It is now possible to render a surface on the edge of a neutron star based on the 3D-data obtained from computer simulations. It is also now possible to show the individual components of the magnetic field of such a simulation, in both 2D and 3D, but this component doesn't work perfectly yet and could be improved in the future.

This program was then used to research the merging of colliding neutron stars, with the help of simulation data. Neutron stars are stars with very high densities, which consist almost completely of neutrons. When two neutron stars merge, either a black hole forms immediately, or a neutron star forms temporarily which will become a black hole after a short time. Specifically, the composition of the matter ejected after the collision was researched. The extremely strong magnetic field of the neutron stars creates a stream of matter which is ejected at the magnetic poles of the neutron star.

This research investigated whether the ejected matter forms nuclei of high or low mass. If mostly nuclei of low mass are formed, they cause the emission of mostly ultraviolet and visible light, but if heavier nuclei are formed, mostly infrared light is emitted. The research has shown that the matter ejected at the magnetic poles mostly form lighter nuclei, so they could be a possible source of the ultraviolet light we have received from merging neutron stars.